Sound Out the Deep Clarity: Super-resolution Photoacoustic Imaging at Depths

Nanchao Wang and Junjie Yao, *Member, IEEE*

***Abstract*—Photoacoustic imaging (PAI), also known as optoacoustic imaging, is a hybrid imaging modality that combines the rich contrast of optical imaging with the deep penetration of ultrasound imaging. Over the past decade, PAI has been increasingly utilized in biomedical studies, providing high-resolution high-contrast images of endogenous and exogenous chromophores in various fundamental and clinical research. However, PAI faces challenges in achieving high imaging resolution and deep tissue penetration simultaneously, limited by the optical and acoustic interactions with tissues. Overcoming these limitations is crucial for maximizing the potential of PAI for biomedical applications. Recent advances in super-resolution PAI have opened new possibilities for achieving high imaging resolution at greater depths. This review provides a comprehensive summary of these promising strategies, highlights their representative applications, envisions the potential future directions, and discusses the broader impact on biomedical imaging.**

***Index Terms*— Photoacoustic imaging, optoacoustic imaging; super-resolution imaging, deep-tissue imaging**

I. Introduction

Photoacoustic (PA) imaging (PAI) is a hybrid technology that synergizes optical imaging and ultrasound (US) imaging to provide high-resolution, high-contrast images of biological tissues [1-5]. Compared to other imaging modalities, PAI can offers greater imaging depth than optical microscopy modalities (e.g., optical coherence tomography and confocal microscopy), better functional and molecular sensitivity than conventional ultrasound imaging, and uses non-ionizing radiation unlike X-ray CT and PET/SPECT. Despite its relatively short history in biomedical imaging, PAI has rapidly advanced in the last decades, driven by its capabilities of multi-scale imaging that spans from organelles and cells to tissues and organs [2, 3, 6]. Based on its imaging principles, PAI can be classified into two categories: photoacoustic microscopy (PAM) and photoacoustic computed tomography (PACT). PAM is further grouped into optical-resolution PAM (OR-PAM) and acoustic-resolution PAM (AR-PAM) [3]. OR-PAM provides the best imaging resolution and operates in the optical ballistic regime, by tightly focusing the laser beam within one optical transport mean free path (~1 mm in soft tissues) [3, 7]. In contrast, AR-PAM functions in the optical diffusive regime by focusing the acoustic detection, allowing for greater penetration depths (~3-5 mm) [3, 8]. PACT uses wide-field optical excitation with diffused light illumination and US transducer arrays to acquire data simultaneously, achieving rapid cross-sectional or volumetric imaging at centimeter-level penetration depth [2, 5]. The generated acoustic waves from the imaging target are processed with various image reconstruction algorithms (e.g., delay-and-sum, filtered back projection, model-based reconstruction, time reversal, etc.) [9].

Despite its impressive development over decades, PAI faces several physical and practical challenges. One major challenge is the tradeoff between imaging resolution and penetration depth [3, 5, 6]. OR-PAM can achieve optical diffraction-limited resolution (micrometer level) to reveal fine structures of organelles and cells, but it is confined to a relatively superficial region of biological tissue (approximately 1 mm of depth). AR-PAM, with its ability to penetrate a few millimeters into tissue,

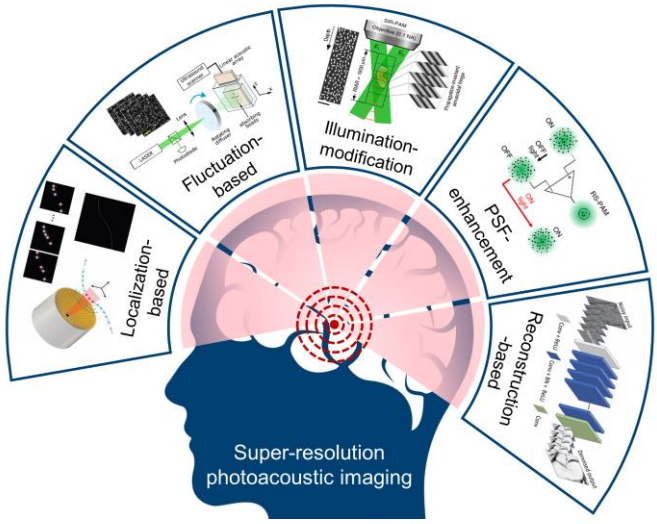

Fig. 1. Summary of different strategies for super-resolution photoacoustic imaging (SR-PAI).

This work was partially sponsored by the United States National Institutes of Health (NIH) grants R21EB027981, R21 EB027304, RF1 NS115581, R01 NS111039, R01 EB028143, R01 DK139109; The United States National Science Foundation (NSF) CAREER award 2144788; Duke University Pratt Beyond the Horizon Grant; Eli Lilly Research Award Program; and Chan Zuckerberg Initiative Grant (2020-226178).

Nanchao Wang is affiliated with Department of Biomedical Engineering, Duke University, Durham, NC 27708 (e-mail: nanchao.wang@duke.edu).

Junjie Yao is affiliated with Department of Biomedical Engineering, Duke University, Durham, NC 27708 (e-mail: junjie.yao@duke.edu).

Highlights

- **This review presents a comprehensive summary of super-resolution photoacoustic imaging (SR PAI) methods.**
- **Representative methods are included: localization-based methods, fluctuation-based methods, illumination-modification-based methods, PSF-enhancement-based methods, and reconstruction-based methods.**
- **This paper highlights the corresponding applications, envisions the potential future directions, and discusses the broader impact on biomedical imaging.**

provides detailed information on deep vascular networks or surface organs of small animals and humans, although its lateral resolution (tens of μm) is inferior to that of OR-PAM. PAM techniques often suffer from degraded resolutions in out-of-focus regions [3]. PACT can perform deep tissue imaging at centimeter depth beyond the reach of typical optical imaging modalities. However, the spatial resolution of PACT is usually worse than PAM, ranging from a few hundred micrometers to millimeters [2, 5]. This resolution limitation is mainly limited by the inherent acoustic diffraction and the transducer geometry. Thus, the resolution of PAI is approximately limited by the optical diffraction for OR-PAM or the acoustic diffraction for AR-PAM and PACT. In practice, it is challenging for a PAI implementation to achieve both high resolution and deep penetration. Achieving super-resolution (SR) at depths is thus highly desired for advancing various biomedical applications of PAI. In this review, we summarize recent advances in super-resolution PAI research, particularly for imaging deep biological tissues, including localization-based methods, fluctuation-based methods, illumination-modification-based methods, PSF-enhancement-based methods, and reconstruction-based methods (Fig. 1). We provide an overview of their technological strategies, and discuss future directions.

II. Localization-based Methods

Inspired by localization-based super-resolution fluorescence imaging techniques [10, 11], ultrasound localization microscopy (ULM) has enabled sub-diffraction images of microvascular structures in deep tissues [12]. Similarly, localization techniques can be adapted by PAI to achieve super-resolution [13]. Localization-based SR-PAI tracks the central positions of flowing agents in the blood vessels that are smaller than system's spatial resolution. Successful application of this technique requires the exogenous or endogenous contrast agents to be small enough to navigate narrow microvessels and sparsely distribute to minimize overlapping, which would otherwise degrade the image quality. Additionally, these agents must produce strong PA signals that stand out against background tissues. Balancing the sparsity of the contrast agents with high signal-to-noise ratio (SNR) is crucial for localization-based SR-PAI. Both exogenous and endogenous contrast agents have been explored by localization-based SR-PAI.

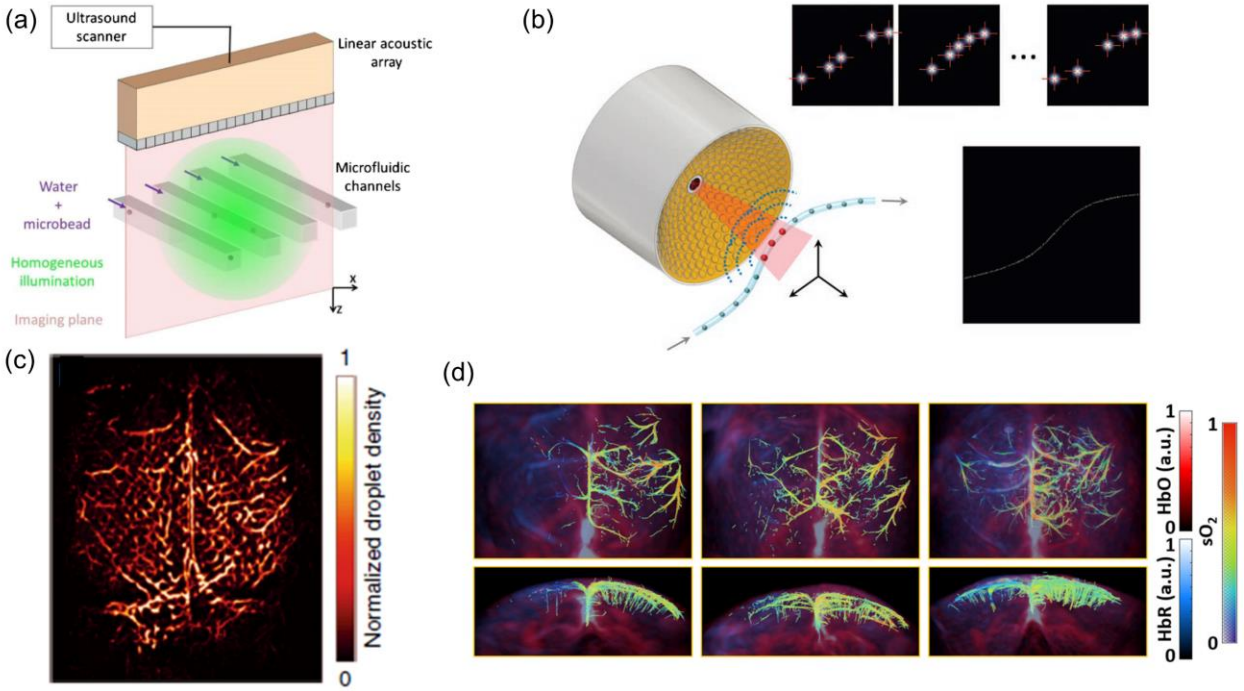

Fig. 2. Localization-based SR-PAI methods using exogenous contrast agents. (a) Localization-based method with a linear transducer array on microfluidic channel [14]. (b) Illustration of 3D localization-based PACT system using a hemispherical transducer array [13]. (c) *In vivo* localization PACT image of a mouse brain [15]. (d) Measurement of blood oxygenation in a stroke mouse brain by 3D localization PACT [16].

A. Exogenous contrast agent

In 2017, Vilov *et al.* first demonstrated the feasibility of using exogenous contrast agents for SR-PACT [14]. They localized individual optical absorbers to achieve 2D super-resolution imaging beyond the acoustic diffraction limit. This proof-of-concept study was performed using a microfluidic channel system with 10-μm absorbing beads mimicking blood vessels (Fig. 2a). A 15 MHz linear capacitive micromachined ultrasonic transducer array acquired 2D PACT images, and by localizing individual absorbers, they achieved a spatial accuracy of better than 1/10 of the acoustic wavelength. Furthermore, Deán-Ben *et al.* extended this idea to 3D PACT using a 2D transducer array [13], where sparsely distributed 30-μm absorbing microspheres were used as the tracking targets (Fig. 2b). A 220-μm diameter knot was imaged by a 256-channel 4-MHz spherical 2D transducer array. While the knot was not resolved in the conventional PACT image, the localization PACT clearly delineated the knot shape. Notably, the localization images not only showed significant improvements in spatial resolution but also enhanced the visibility of limited-view structures.

The first in-vivo localization PACT of mouse brain cortical vessels was demonstrated by Zhang *et al.* in 2019 [15]. Using a 512-channel 5-MHz ring-array, they employed dyed droplets filled with near-infrared dye IR-780 iodide (Fig. 2c). The dye had a molar extinction coefficient 300 times greater than that of hemoglobin at 780 nm, facilitating the localization of isolated droplets. This technique enabled the separation of vessels 25 μm apart, achieving a six-fold improvement in spatial resolution.

Continuing this effort, Deán-Ben *et al.* employed a 512-channel 2D transducer array for imaging in-vivo mouse brain with ischemic stroke [16]. They used 5-μm dichloromethane-based microdroplets with optical absorption several orders of magnitude higher than that of hemoglobin at near-infrared wavelengths, enabling single-particle localization *in vivo*. This approach resulted in non-invasive 3D microangiography of the mouse brain with a resolution better than 20 μm. Functional imaging of blood oxygenation and blood flow was also demonstrated (Fig. 2d), showing a significant decrease in microvascular density and flow speed induced by ischemic stroke.

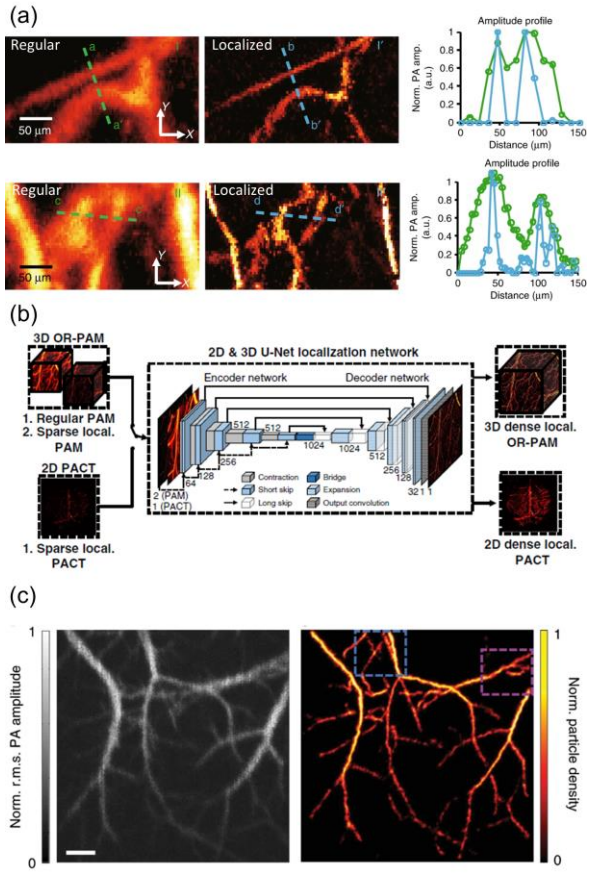

Fig. 3. Localization-based SR-PAI methods using endogenous contrast agents. (a) Comparisons of the vascular images by traditional OR-PAM and RBC localization OR-PAM [17]. (b) Illustration of 2D and 3D U-Net network architecture for localization OR-PAM and PACT [18]. (c) Comparison of the vascular image by traditional OR-PAM (left) and melanin localization OR-PAM (right) [19].

B. Endogenous contrast agent

Red blood cells (RBCs) can also be used as localization targets to enhance the spatial resolution of PAI. In 2019, Kim *et al.* applied the localization OR-PAM technique to improve resolution and overcome the limited depth-of-focus [17]. Taking advantage of the high signal to noise ratio (SNR) and high frame rate, OR-PAM images captured the locations of individual RBCs, achieving a 2.5-fold improvement in spatial resolution *in vivo* (Fig. 3a). To address the limited temporal resolution of the localization approach, Kim *et al.* proposed a deep neural network technique to enhance the tracking speed of localization OR-PAM (Fig. 3b) [18]. This method allowed for constructing SR images with fewer raw images, which is also applicable for localization PACT.

Besides, the strong optical absorption of melanin at ~660 nm provides high contrast over the background signals, which can be used for tracking and localizing circulating melanoma cells. In 2020, Yang et al. reported a high-speed photoacoustic topography with an ergodic relay, providing high-throughput wide-field volumetric imaging with a single-element ultrasound detector [19]. In this work, tracking and localizing flowing melanoma cells was demonstrated in the mouse brain in vivo (Fig. 3c), leveraging the high imaging speed of the system. This technique enabled the separation of vessels 300 nm apart, an 83-fold improvement in spatial resolution.

III. Fluctuation-based methods

Originally developed to improve the resolution of conventional fluorescence microscopy, the statistical analysis of temporal signal fluctuations provides a novel way to achieve sub-diffraction resolution. This method, known as super-resolution optical fluctuation imaging (SOFI) [20], has since been adapted for SR-PAI. Specifically, analyzing high-order fluctuations in PA signals can resolve optically absorbing structures beyond the acoustic diffraction limit. Signal fluctuations can be introduced by two methods: external speckle illumination and fluctuating signal sources.

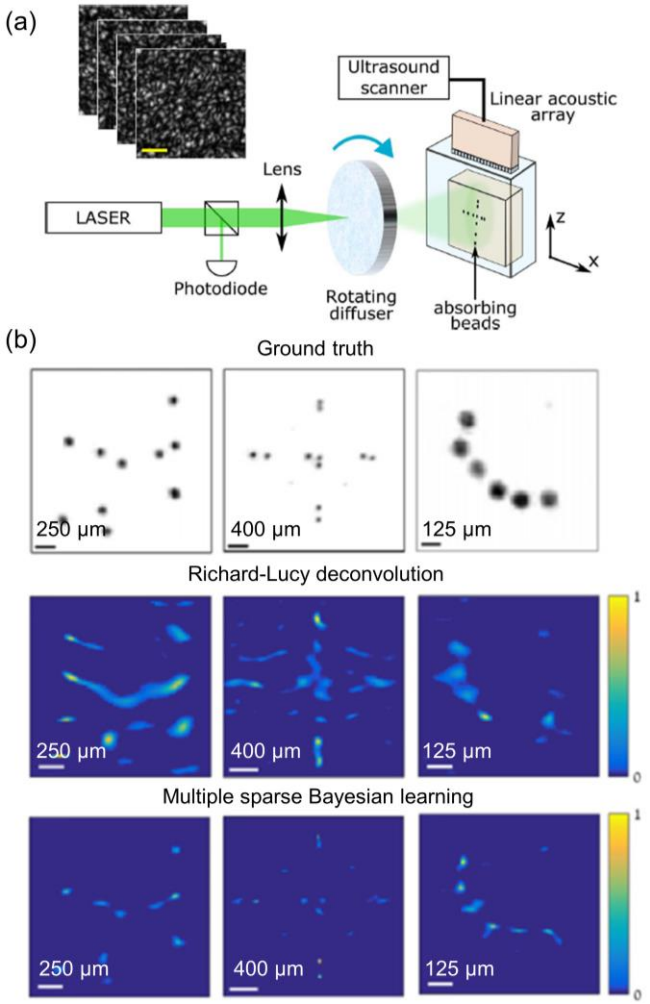

Fig. 4. Fluctuation-based SR-PAI methods using external speckle illumination. (a) Typical system setup for external speckle illumination [23]. (b) Experimental comparison of reconstruction strategies for external speckle illumination [26]. First row: Optical images of the absorbing beads without any scattering. Second row: Reconstructed 2nd-order fluctuation image followed by Richardson-Lucy deconvolution. Third row: Reconstructed fluctuation images using the multiple sparse Bayesian learning method.

A. External speckle illumination

In optical imaging, using external speckle illumination to introduce signal fluctuations is a common practice [21]. The statistical analysis of signal fluctuation typically involves calculating high-order statistical moments, such as the second or third cumulants, of the fluctuated signal intensity over time. For PAI, multiple speckle illumination was first introduced by Gateau *et al.* in 2013 [22], although no SR-PAI was demonstrated in this initial work. The first demonstration of SR-PAI using speckle illumination was reported by Chaigne *et al.* in 2016 [23]. They generated scattered light by rotating a ground glass diffuser to illuminate black polyethylene beads embedded in an agarose gel block (Fig. 4a). Using a 4-MHz, 128-channel linear array, they experimentally showed that second-order signal fluctuations in PAI improved resolution by about 1.4 times for sparsely distributed beads.

Murray *et al.* later presented a similar method for enhancing PAI spatial resolution with speckle illumination [24]. Randomized speckle patterns were produced by a rotating optical diffuser. The reconstruction method exploited the joint sparsity of sound sources. Using a single 90-MHz focused transducer and a translation stage, their experiments with alpaca fibers showed a resolution enhancement of at least two times. Liu *et al.* investigated the theoretical resolution limit for this method, demonstrating that >2-fold improvement could be achieved with tailored super-Rayleigh speckle [25]. Notably, conventional SOFI with high-order statistical analysis can introduce significant artifacts with insufficient image frames. Hojman *et al.* proposed an approach using dynamic speckle illumination combined with a compressed sensing computational reconstruction framework [26]. This method considered the system response and target sparsity. Their results showed that this compressed sensing method not only enhanced spatial resolution but also reduced the required number of frames, offering advantages over conventional high-order SOFI (Fig. 4b). However, no *in-vivo* SR-PAI based on external speckle imaging has been reported to date. One

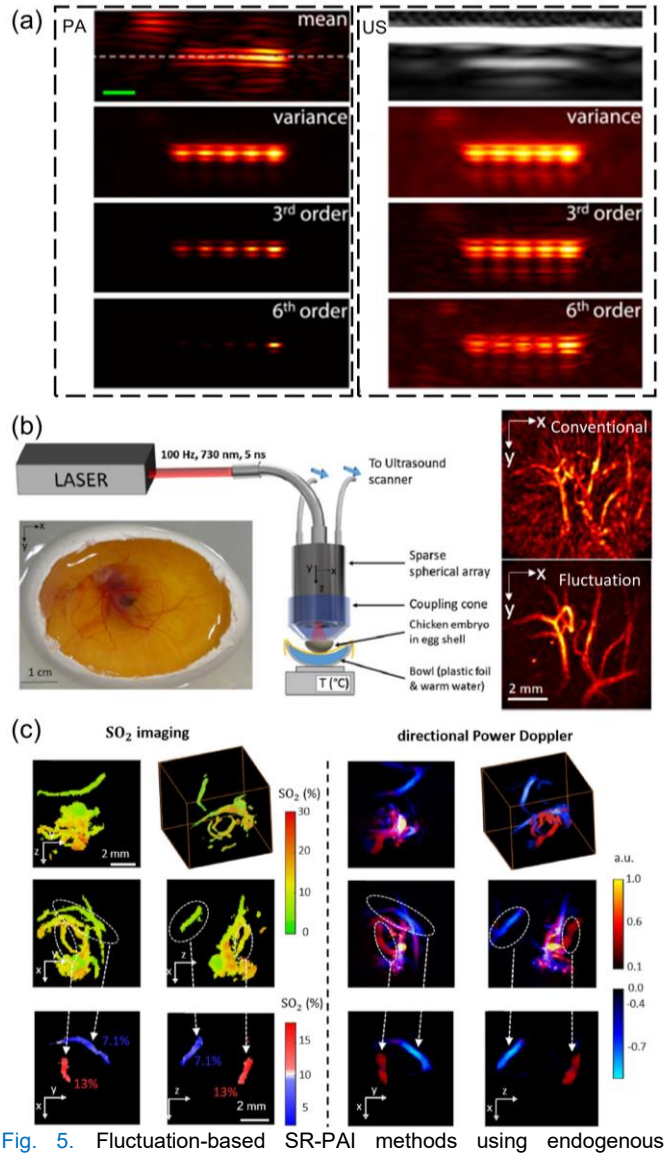

Fig. 5. Fluctuation-based SR-PAI methods using endogenous fluctuating sources. (a) Experimental results of microfluidic circuit with flowing absorbing particles [27]. (b) Experimental setup and results for 3D *in vivo* imaging of a chicken embryo [28]. (c) sO_2 imaging and directional power doppler imaging of chicken embryo [29].

challenge is the strong scattering of biological tissues, which results in the fully-developed speckles at the scale of optical wavelengths. Such fine speckle patterns may not introduce detectable signal fluctuations.

B. Endogenous fluctuating sources

Surpassing the acoustic diffraction limit by exploiting inherent temporal fluctuations, such as those induced by the flowing RBCs, is also possible. Chaigne *et al.* first demonstrated the potential for SR-PAI through numerical and phantom studies [27]. The flowing particles and whole human blood enabled contrast-agent-free resolution improvement and background reduction. Experimental demonstrations included imaging parallel microfluidic channels with absorbing particles or whole human blood with physiological concentrations (Fig. 5a).

In 2020, Vilov *et al.* provided the first *in vivo* demonstration of SR-PAI by leveraging the randomness introduced by RBC flowing [28]. Concurrently, theoretical predictions and Monte Carlo simulations demonstrated that second-order fluctuation images could significantly mitigate the limited-view issues. Using a customized 256-channel spherical transducer array operating at 8 MHz, they acquired 768 in-situ images of the microvasculature in a chicken embryo chorioallantoic membrane model (Fig. 5b). Fluctuation images with prior singular value decomposition (SVD) filtering showed resistance to pulse energy fluctuations in both simulations and experiments. Typically, the largest singular values correspond to clutter signals (slow-moving blood or stationary tissue), while smaller singular values are associated with blood flow (fast-moving blood). Godefroy *et al.* expanded the similar concept to multispectral photoacoustic fluctuation imaging to enable quantitative molecular imaging, such as measuring blood oxygenation [29]. They also integrated ultrasound power Doppler imaging to provide complementary information about blood flow dynamics. Using a sparse linear transducer array with 256 elements, the in-vivo experiments on chicken embryos demonstrated enhanced resolution and contrast in both ultrasound and photoacoustic images of blood vasculature. This included oxygen saturation and directional power Doppler information (Fig. 5c). The lateral and axial resolution of traditional PAI are 0.18 mm and 0.27 mm, respectively. The resolution of fluctuation-based SR PAI is improved by $\sqrt{2}$ according to the SOFI theory [29].

IV. Illumination-Modification-Based Methods

The PAM's lateral resolution degrades significantly outside the depth of focus (DoF) of the optical or acoustic beam [3]. In Gaussian beam-based OR-PAM, there is an inherent trade-off between lateral resolution and DoF. Similarly, acoustic diffraction limits the lateral resolution of AR-PAM. To address these challenges, various illumination-modification methods have been proposed to extend the DoF while maintaining lateral resolution for PAM. Technically speaking, external speckle imaging could also be categorized as illumination-modification-based methods. However, almost all implementations of the external speckle imaging primarily aim for resolution enhancement for PACT rather than improving DoF for PAM, and it relies more on the stochastic analysis of fluctuating signals.

A. Structured illumination

Structured illumination is a well-known super-resolution technique widely used in optical microscopy [30, 31]. In PAM, structured illumination helps overcome limitations by down-converting high-frequency spatial components into the system's passband. The first structured-illumination PAM system was demonstrated by Liang *et al.* in 2014 using a digital micromirror device (DMD) [32], inspired by the spectral Fourier-multiplexing method [33]. The DMD served as an illumination pattern encoder to produce discrete Fourier modulation patterns for each spatial element, enabling the decoding of the spatial distribution of optical absorption.

Yang *et al.* proposed a new technique called motionless volumetric spatially invariant resolution PAM [34], which combines 2D Fourier-spectrum optical excitation with single-element depth-resolved PA (Fig. 6a). The propagation-invariant sinusoidal fringes generated by the DMD achieved the spatially-invariant lateral resolution. Amjadian *et al.* proposed a similar structured-illumination PAM system [35]. Later, Amjadian *et al.* proposed a modified structured

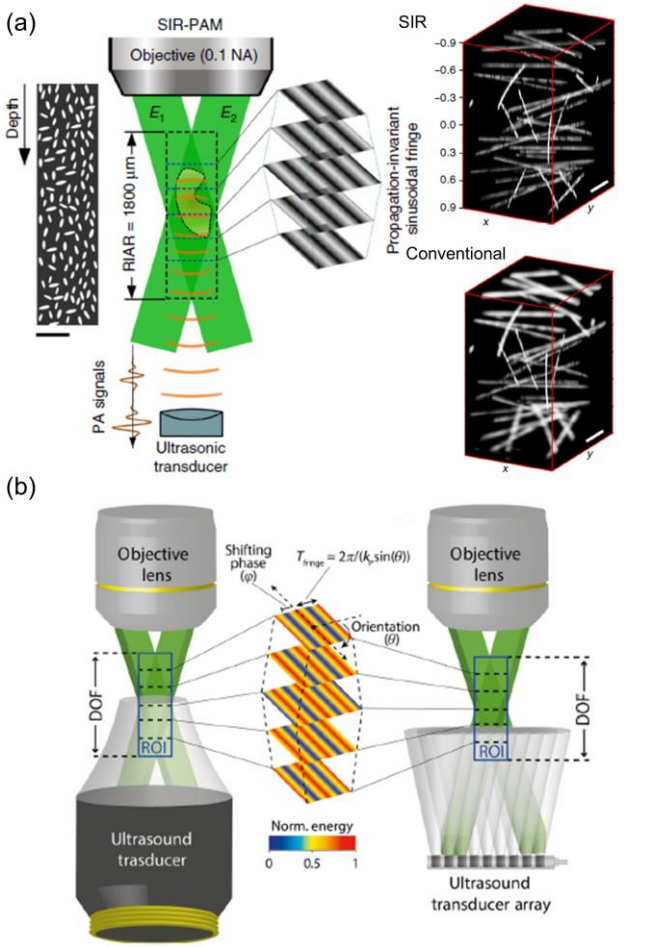

Fig. 6. Illumination-modification-based SR-PAI methods using structured illumination. (a) Principle of motionless spatial invariant resolution (SIR) PAM and the images of carbon fibers by SIR-PAM and conventional PAM (right column) [34]. (b) Comparison of illumination schemes between original SIR-PAM and the modified SIR-PAM with phase-shifting [36].

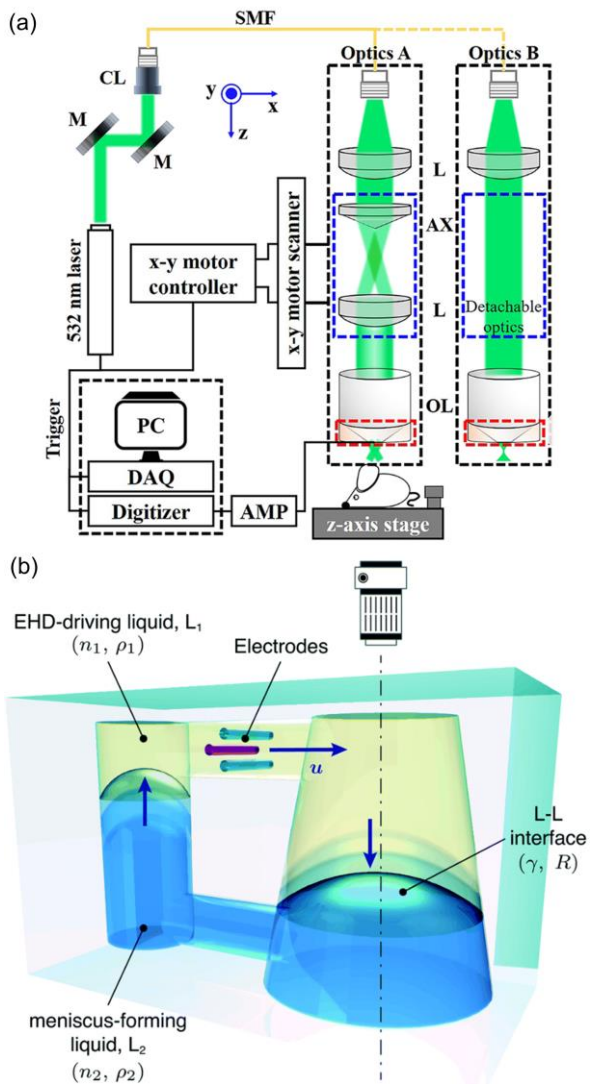

Fig. 7. Illumination-modification-based SR-PAI methods using Bessel beam and focus-shifting lens. (a) Schematic diagram of the reflection-mode switchable subwavelength-resolution Bessel-beam and Gaussian-beam PAM [40]. AX, axicon lens; CL, collimator; L, lens; M, mirror; OL, objective lens; OS, optical system; SMF, single-mode-fiber; (b) Schematic of the dielectro-optofludic lens (DOL) [43]. EHD, electrohydrodynamic.

illumination setup to improve the lateral resolution alongside depth of view and imaging speed [36]. In this setup, instead of single-position focused illumination, plane wave illumination was adopted, and its amplitude was modulated with sinusoidal fringes to enhance the captured spectrum and lateral resolution (Fig. 6b). Consequently, the resultant acoustic pressure waves were acquired by a 2D planar transducer array. Another structured-illumination PAM was reported by modifying the phase-shifting method in 2022 [37]. Structured-illumination with a three-phase-shifting method can improve the resolution by two folds. Here, a modified three-phase-shifting method is used to generate the second harmonics of the fringes and double the spectral shift.

Multifocal structured illumination PAM was proposed by Chen et al. that involves using a grid of focused optical spots to illuminate the tissue surface [38]. It combined the illumination method of PAM (multiple focal spots scanned with an acousto-optic deflector) with the detection method of PACT (semispherical transducer array) to accelerate the imaging speed. The multifocal illumination pattern is generated by a beam splitting grating, and the images are subsequently formed by inverse reconstruction methods. Multifocal structured illumination PAM has achieved high-resolution, high-speed, and wide-field imaging with a lateral resolution of 28 μm and an imaging speed of 12.5 s.

B. Bessel beam

The Bessel beam, generated by an axicon lens, generally offers a longer DoF than a Gaussian beam and maintains a consistent lateral resolution over an extended depth range. This makes Bessel beams advantageous for enhancing image resolution in the out-of-focus regions. The Bessel-beam-based PAM system can be easily modified from a Gaussian-beam-based PAM by replacing the optical illumination setup [39, 40]. Park *et al.* developed a reflection-mode switchable subwavelength Bessel-beam and Gaussian-beam PAM system (Fig. 7a), confirming that the DoF of Bessel-beam PAM is significantly longer than that of Gaussian-beam PAM. However, a major drawback of Bessel-beam PAM is the strong sidelobes. To address this issue, blind deconvolution and Grüneisen relaxation effect were employed. Using these methods, Jiang *et al.* and Park *et al.* extended the DoF of OR-PAM from 65 μm and 33 μm to 483 μm and 229 μm, respectively [39, 40]. Shi *et al.* further achieved a DoF of 1600 μm while maintaining a 6.1 μm lateral resolution [41] by leveraging the Grüneisen relaxation effect.

C. Focus-shifting lens

A conventional approach to address the short DoF issue in OR-PAM is to mechanically shift the optical focus. However, this method often decreases the imaging speed [42]. To overcome this, Kim *et al.* proposed to use a dielectro-optofluidic lens (DOL) that can change its focal length by electrically adjusting the lens-acting liquid level (Fig. 7b) [43]. This method demonstrated an extended DoF and maximized the PA signal through focal length adjustments. Another technique is to use a tunable acoustic gradient (TAG) lens, which can swiftly change its effective focal length. In 2017, Yang *et al.* demonstrated an OR-PAM system utilizing a TAG lens to extend the DoF to 750 μm [44]. The TAG lens consists of a cylindrical piezoelectric shell filled with silicone oil, with its focal length adjustable according to the applied sinusoidal signal.

V. PSF-ENHANCEMENT-BASED METHODS

Biological tissue can distort the optical wavefront and cause optical aberration as light propagates through, making it challenging to maintain high spatial resolution in PAM of deep tissues. Large aberrations in high numerical-aperture objective lenses exacerbate this issue. Since the performance of OR-PAM depends on the quality of the system's point spread function (PSF), it suffers from degradations in both PA signal amplitude and spatial resolution when imaging at depths. To address these challenges, adaptive optics (AO) and other PSF-enhancement techniques have been introduced to improve image quality. Generally, AO not only helps to improve lateral resolution but also enhances the imaging contrast by narrowing

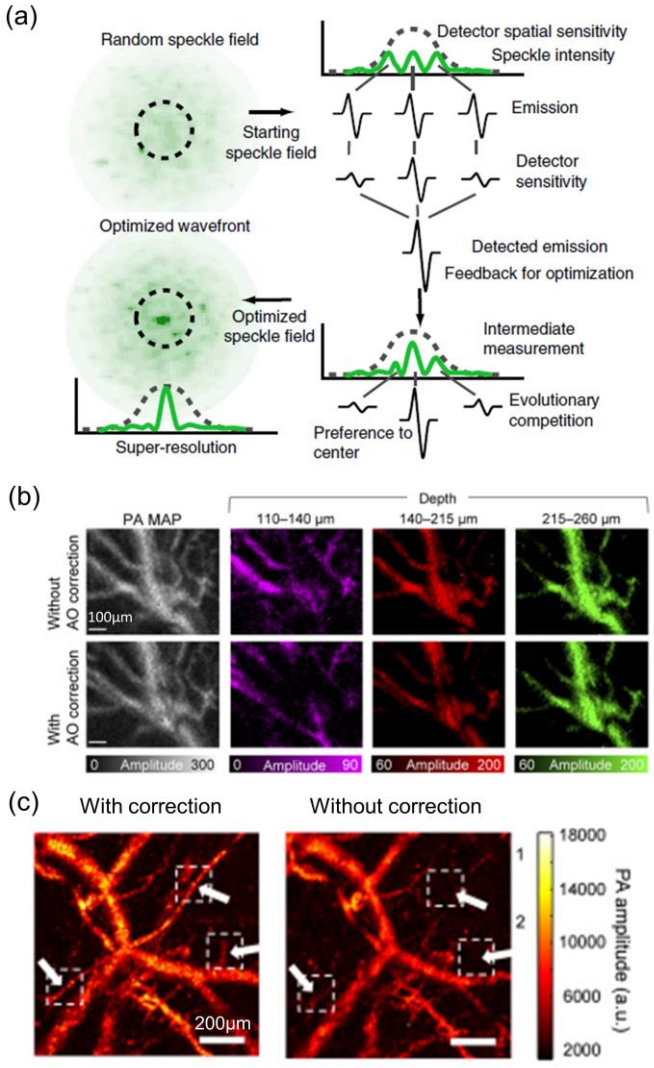

Fig. 8. PSF-enhancement-based SR-PAI methods using adaptive optics. (a) Illumination of optical focus creation with photoacoustic feedback [47]. (b) *In vivo* OR-PAM image of mouse ear image based on the transmissive adaptive optics [48]. (c) *In vivo* mouse ear image generated from acoustic-feedback wavefront-adapted PAM [49].

optical focus. Additionally, using photoswithchable chromophores or non-linear optical effects can also help highlight the center of PSF via differential signals.

A. Adaptive optics

The first report to introduce AO into OR-PAM was published in 2010 [45], aiming to correct the wavefront distortions of the illuminating light. This was achieved by using a close-loop AO system consisting of a 141-element MEMS-based deformable mirror and a Shack-Hartmann wavefront sensor operating at 15 Hz. This setup achieved a lateral resolution of better than 2.5 μm using a low NA objective lens. In 2013, Caravaca-Aguirre *et al.* demonstrated transmissive AO OR-PAM through a scattering medium [46], by using a spatial light modulator to control the input light wavefront. Conkey *et al.* further demonstrated SR-PAI through a scattering wall using photoacoustic signal as the feedback for wavefront optimization (Fig. 8a) [47], showing improved resolutions in ex vivo samples. In 2022, Notsuka implemented *in vivo* OR-PAM imaging based on transmissive AO [48]. The system used a

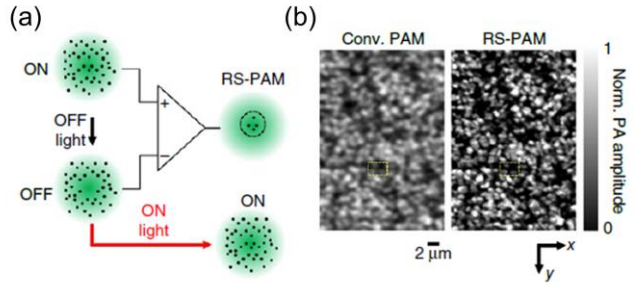

Fig. 9. PSF-enhancement-based SR-PAI methods using photoswitching [51]. (a) Principle of reversibly switchable PAM (RS-PAM). (b) Conventional (conv.) PAM and RS-PAM images of BphP1-expressing bacteria densely fixed on a coverslip, showing the superior lateral resolution of RS-PAM.

low-frequency ultrasound transducer with a compact transmissive AO device. The AO device is composed of three layers of liquid-crystal molecules sandwiched between glass substrates. This setup improved lateral resolution by 115% in the mouse ear (Fig. 8b). In 2024, Shen *et al.* developed acoustic-feedback wavefront-adapted PAM to dynamically compensate for tissue-induced light aberration at depths in zebra fish embryos and mouse ears (Fig. 8c) [49].

B. Photoswitching

Reversibly switchable fluorescent proteins can be alternated between a fluorescent and nonfluorescent state by varying the excitation wavelengths, resulting in improved spatial resolution in localization-based fluorescence imaging. This technique can be exploited in PAI to improve the contrast-to-background ratio and spatial resolution by modulating the signals of labeled tissues.

Stiel *et al.* first reported reversibly switchable fluorescent proteins (Dronpa and the variant Dronpa-M159T) in PAT in 2015 [50]. They modulated PA signals to increase the contrast-to-noise, although this work did not demonstrate resolution enhancement. In 2016, Yao *et al.* demonstrated the use of a reversibly switchable non-fluorescent bacterial phytochrome, BphP1, for super-resolution PAI [51]. This method combined OR-PAM with efficient BphP1 photoswitching, which enabled differential imaging with substantially improved spatial resolution (Fig. 9a). In this work, a series of Gaussian-shaped laser pulses at 780 nm repeatedly strike a group of ON-state BphP1 molecules, the PA signals generated by the consecutive laser pulses decrease in amplitude as more BphP1 molecules are switched off at a rate proportional to the local excitation intensity. The PA signal from the center of the excitation spot decays faster than that from the periphery, accentuating the contribution from the center. This approach was able to suppress the PA signals generated by the out-of-focus regions and consequently achieved an axial resolution of ~0.4 μm, ~75-fold finer than that of conventional OR-PAM (Fig. 9b).

C. Nonlinear effect

A nonlinear effect frequently used in SR-PAI is the temperature-dependent Grüneisen coefficient. The first implementation of Grüneisen relaxation PAM (GR-PAM) was reported by Wang *et al.* in 2014 [52], improving the axial resolution from 45 μm to 2.3 μm and the lateral resolution from 0.63 μm to 0.41 μm. GR-PAM delivers two identical laser

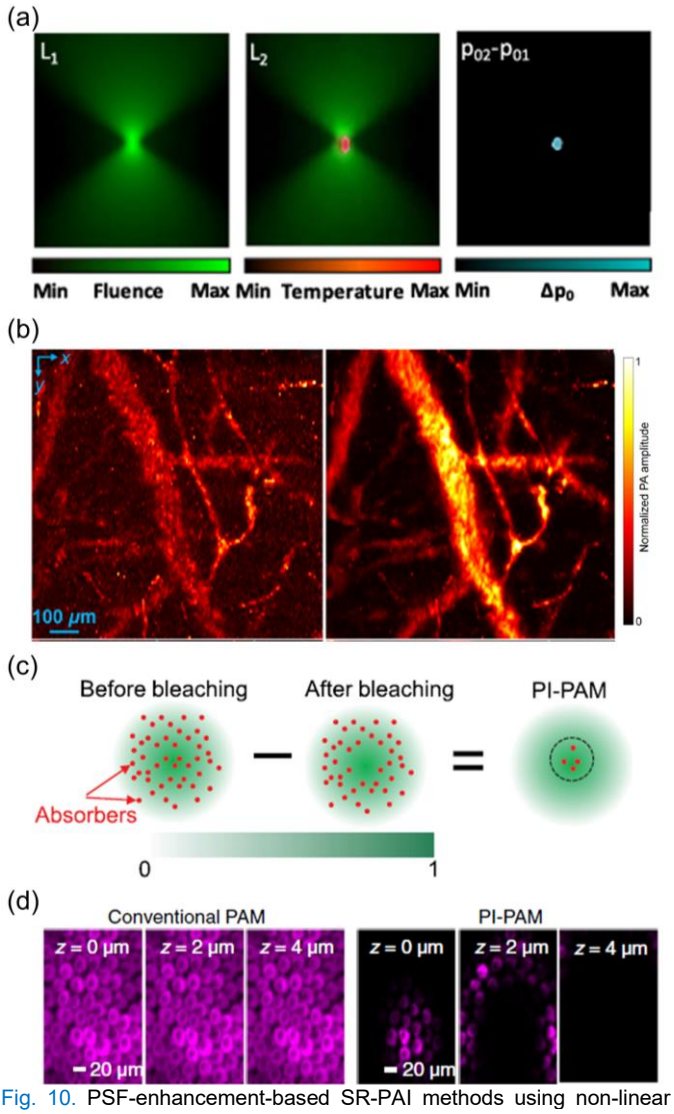

Fig. 10. PSF-enhancement-based SR-PAI methods using non-linear effects. (a) Principle of Grüneisen relaxation PAM (GR-PAM) [52]. (b) Representative GR-PAM results of *in vivo* mouse brain [53]. (c) Principle of photoimprint PAM (PI-PAM) [57]. (d) Representative PI-PAM results of rose petal cells at different depths [57].

pulses with a microsecond delay, and detects the amplitude difference between the two photoacoustic signals (Fig. 10a). The first laser pulse generates a photoacoustic signal and increases the temperature of the in-focus absorbers. When the second laser pulse excites the thermally-tagged absorbers within the thermal relaxation time, a stronger photoacoustic signal is produced due to the temperature dependence of the Grüneisen coefficient. The signal difference highlights the contribution from the optical focus and thus improve the axial resolution. Alternatively, a continuous-wave (CW) laser can be used for the thermal tagging between the two laser pulses, which was demonstrated for *in vivo* mouse brain imaging, with significant improvement in image contrast and axial resolution (Fig. 10b) [53]. Liu *et al.* demonstrated ultraviolet GR-PAM to provide better contrast in mouse brain slice, achieving 15-μm axial resolution and 0.64-μm lateral resolution [54]. Another application of GR-PAM is to use ultraviolet thermal tagging to suppress the mid-infrared (MIR) absorption of water in fresh biological samples. Shi *et al.* introduced this idea in 2019 and achieved background-free MIR imaging of lipids and proteins with ultraviolet resolution, at least an order of magnitude finer than the MIR diffraction limit [55]. Shi *et al.* also demonstrated that an 8.26-fold contrast enhancement is achieved for imaging swine-adipose tissue at 1.7 μm in comparison to conventional PAM [56].

Photobleaching is another nonlinear effect explored for SR-PAI. In 2014, Yao *et al.* introduced photoimprint PAM (PI-PAM), based on the nonlinear photobleaching process [57]. In PI-PAM, when a sample is illuminated by an excitation laser beam, absorbers undergo photobleaching with a bleaching rate depending on the local optical fluence. The differential image before and after photobleaching highlights the center of the optical focus (Fig. 10c). The lateral resolution was improved from 200 nm to 120 nm with an oil-immersion objective lens at 532 nm (Fig. 10d). Nevertheless, the photobleaching process is damaging to the samples, and may generate toxic radicals, such as reactive oxygen species, potentially interrupting cellular processes and jeopardizing cell viability.

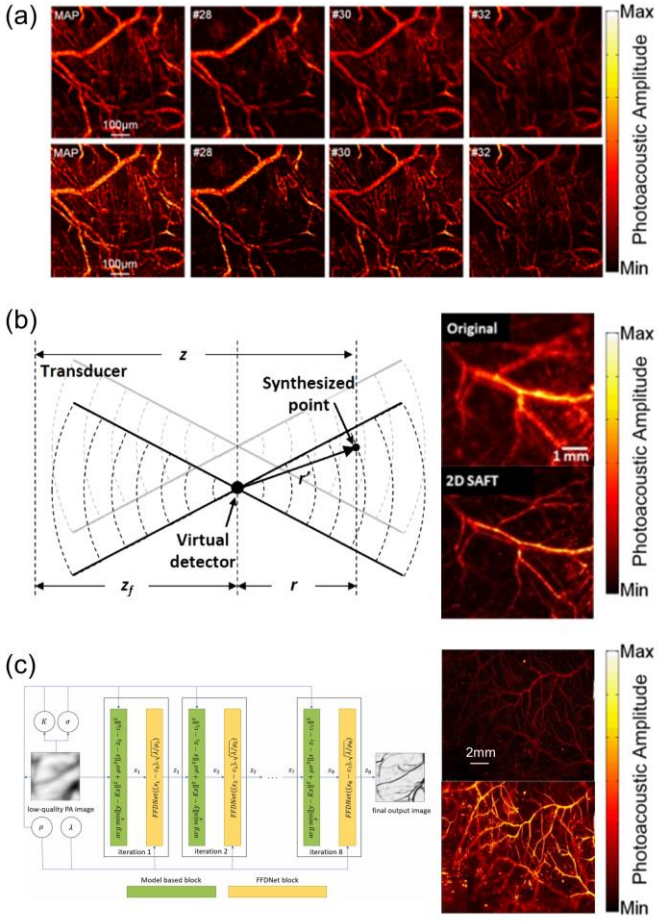

Fig. 11. Reconstruction-based SR-PAI methods. (a) Representative OR-PAM images before (top row) and after blind deconvolution (bottom row) [63]. MAP: maximum amplitude projection. Number on the top left corner refers to different depths. (b) Principle of synthetic aperture focusing (SAFT, left) and the comparison between conventional AR-PAM and 2D directional SAFT AR-PAM (right) [71]. (c) Workflow of the model-based and learning-based model (left) as well as the comparison between conventional and the improved algorithms [77].

VI. Reconstruction-based Methods

Reconstruction-based methods can enhance the resolution of PAI without modifying the hardware, by leveraging advanced

mathematical, statistical, and machine learning techniques. However, most reconstruction-based SR-PAI methods rely on *a priori* knowledge or assumptions about the system's PSF, which may not be available or reliable in practice. Additionally, deep learning techniques may introduce 'hallucination' due to the model complexity and lack of training data.

A. Deconvolution

Deconvolution-based image enhancement methods have been explored for PACT [58], OR-PAM [59], and AR-PAM [60]. Typical deconvolution methods, including Richardson-Lucy (RL) deconvolution [61] and model-based deconvolution [62], usually require *a prior* knowledge of the system PSF, which is often challenging to measure *in vivo*. Without knowing the PSF, blind deconvolution can be used (Fig. 11a) [63]. Because deconvolution-based SR-PAI methods do not require any hardware change, it can be coupled with other reconstruction-based resolution enhancement methods, such as synthetic-aperture focusing [60], and deep convolution neural network [64]. Furthermore, deconvolution is essential to fluctuation-based SR-PAI methods, as high-order fluctuation analysis typically relies on deconvolution.

B. Synthetic aperture focusing technique

Synthetic aperture focusing technique (SAFT) is often used in AR-PAM for enhancing lateral resolution in the out-of-focus region [65]. The lateral resolution degradation of AR-PAM is due to the acoustic focusing rather than the optical focusing. In 2006, Li *et al.* first introduced SAFT in AR-PAM, assembling the PA signals originating from the same source to correct the out-of-focus distortion [66]. Part *et al.* proposed a new SAFT method to further improve the resolution by using the delay-multiply-and-sum algorithm [67]. Meanwhile, several studies have explored 2D or 3D SAFT [68, 69]. However, the out-of-focus lateral resolution was still worse than that within the focus, mainly due to the assumed spherical wavefront. Deng *et al.* proposed an adaptive SAFT method that applies additional 1D SAFT processes in directions perpendicular to each blood vessel [70]. In 2018, Jeon *et al.* presented a new 2D SAFT method that can solve the wavefront mismatch problem (Fig. 11b) [71], by performing independent 1D SAFT in multiple directions.

Table. 1 Representative SR PAI techniques.

Ref.	Method type	PAM/PACT	Experimental spatial resolution	Penetration depth	Imaging time	Major demonstrations in the reference
[16]	Localization-based SR-PAI using exogenous contrast	PACT	20 μm	2.5 mm[1]	5 s	*In vivo* transcranial mouse brain imaging
[17]	Localization-based SR-PAI using endogenous contrast	PAM	Lateral: 0.4-0.7 μm Axial: 2.5 μm	750 μm[2]	1.6 s (single position)	*In vivo m*icrovasculatures PAI in small animals (e.g., mouse ear, mouse eye, mouse brain, etc.)
[23]	Fluctuation-based SR-PAI using external speckle illumination	PACT	140-160 μm	Not applicable	10 s	*Ex vivo* absorbing microbead imaging
[29]	Fluctuation-based SR-PAI using endogenous fluctuating sources	PACT	Lateral: 127 μm Axial: 191 μm[3]	5 mm[4]	~10 s (including multispectral PAI and ultrasound imaging)	*In vivo i*ntegrated 3D sO_2 and Doppler imaging on chicken embryos
[34]	Illumination-modification-based SR-PAI using structured illumination	PAM	Lateral: 1.9 μm Axial: 19 μm	1mm[5]	21 s	*In vivo* zebrafish embryo imaging
[48]	PSF-enhancement-based SR-PAI using adaptive optics	PAM	Lateral: 0.5-0.6 μm Axial: 10.1 μm	1.2 mm[6]	100 ms modulation time + regular OR-PAM acquisition	*In vivo* mouse ear imaging
[51]	PSF-enhancement-based SR-PAI using photoswitching	PAM	Lateral: 0.14 μm Axial: 0.4 μm	45 μm[7]	Not specified	Cancer cell imaging
[53]	PSF-enhancement-based SR-PAI using Grüneisen effect	PAM	Lateral: 0.7 μm Axial: 12.5 μm	150 μm[2]	2.2 h	*In vivo* mouse brain imaging
[57]	PSF-enhancement-based SR-PAI using photoimprint effect	PAM	Lateral: 0.12 μm Axial: 0.4 μm	Not specified	Not specified	Cell imaging (e.g., melanoma cell, blood cell, live rose petal epidermal cell, etc.)
[63]	Reconstruction-based SR-PAI using deconvolution technique	PAM	Lateral: 3.04 μm Axial: not specified	240 μm[8]	Not specified	*In vivo* mouse ear imaging
[71]	Reconstruction-based SR-PAI using SAFT technique	PAM	Lateral: 55 μm Axial: not specified	2 mm[8]	Not specified	*In vivo* mouse ear imaging

[1] Mouse transcranial imaging.
[2] Mouse brain imaging.
[3] Estimated resolutions based on the original PA resolution dividing by $\sqrt{2}$.
[4] Chicken embryo imaging.
[5] Penetration depth underneath chicken breast tissue with optical clearing. See Supplementary Note 7 and Figure 6 in [34].
[6] *Ex vivo* imaging under a glass plate.
[7] BphP1-expressing U87 cell imaging.
[8] Mouse ear imaging.

C. Deep learning

Deep-learning techniques have been widely adopted in optical imaging technologies to improve contrast and spatial resolution, such as confocal microscopy [72], two-photon microscopy [73], fluorescence microscopy [74], and optical coherence tomography [75]. Deep learning methods can also be applied to improve the resolution of PAI. Awasthi *et al.* proposed a deep neural network-based model with the scaled root-mean squared error as the loss function for super-resolution PACT [76]. Feng *et al.* explored CNN-based deconvolution to improve lateral resolution of AR-PAM [64]. Five CNN models were trained for performance comparison, including fully dense UNet, residual channel attenuation network, enhanced deep super resolution network, residual in residual dense block network. The phantom experiments demonstrated a lateral resolution of ~30μm, which was less than half of the original resolution of the AR-PAM system. Zhang *et al.* proposed a framework that combines the model-based and learning-based method in AR-PAM when applied to different imaging depths and frequencies (Fig. 11c) [77]. A deep convolutional neural network was used to implicitly capture the image's statistical and structural information of the vascular targets, which was then incorporated into the model-based framework, enabling adaptive process. *In vivo* results showed significant improvement in SNR and CNR.

VII. Discussion and Conclusion

PAI has been making important contributions to both preclinical and clinical applications, driven by rapid innovations in imaging systems. The unique capability of PAI to acoustically detect optically absorbing targets has provided rich structural, functional, and molecular information of the biological tissues at depths beyond the traditional optical imaging. Despite its technological advances, PAI has the trade-off between the imaging resolution and penetration depths, impeding its broad applicability in deep tissues.

In this concise review, we have summarized different SR-PAI methods to improve the resolution beyond optical or acoustic diffraction. A selective collection of recently developed SR PAI techniques is shown in Table 1. These technological advancements in SR-PAI have opened new possibilities for biomedical research. Despite the significant advancements in SR-PAI, several challenges remain that hinder its widespread application and effectiveness. One primary issue is the limited penetration depth. Many SR-PAI techniques often rely on optical principles that work well near the surface but struggle deeper within biological tissues due to the scattering and absorption of light. This limitation restricts the application of SR-PAI in imaging deeper structures *in vivo*. Another challenge is the complexity and cost of the required equipment. Advanced super-resolution techniques often demand sophisticated setups, including high-speed lasers, specialized detectors, and complex computational algorithms. These requirements can be prohibitively expensive and technically challenging to implement, limiting accessibility to specialized research labs.

The trade-off between resolution and imaging speed is also a significant concern. Achieving super-resolution often necessitates prolonged data acquisition time, which can be impractical for capturing dynamic biological processes. This makes it difficult to apply SR-PAI to live imaging of rapidly changing phenomena, such as neural activity or blood flow. Additionally, the development of suitable contrast agents remains a bottleneck. While nanoparticles and molecular probes have enhanced resolution, for example, in the localization-based methods, their biocompatibility, toxicity, and clearance from the body are critical issues that need to be addressed. The lack of universally applicable and safe contrast agents limits the versatility and clinical translation of SR-PAI.

To overcome these challenges, future research in SR-PAI should focus on several key areas. Enhancing penetration depth is crucial, and can be approached by developing new methods that combine photoacoustic imaging with other modalities, such as ultrasound or magnetic resonance imaging (MRI). These hybrid approaches can leverage the strengths of each modality, providing deeper and more comprehensive imaging. However, integrating different imaging modalities into a single platform may be technically challenging, particularly with different lengths scales. The data fusion from the reconstructed images is also critical to minimize spatial and temporal misalignments.

Simplifying the technological requirements and reducing costs are also vital for broader adoption. Innovations in portable and affordable laser systems, as well as the development of user-friendly software package for image reconstruction, could make SR-PAI more accessible. Additionally, advancements in adaptive optics and wavefront shaping could simplify system design while improving image quality.

Balancing resolution with imaging speed will require new strategies that optimize data acquisition and processing. Compressive sensing and machine learning algorithms hold promise in this regard, as they can reduce the amount of data needed for high-resolution images and accelerate image reconstruction. Developing faster and more efficient computational methods will be essential for real-time super-resolution imaging.

In the realm of contrast agents, research should aim to create biocompatible, non-toxic, and easily cleared agents that can enhance photoacoustic signals. These agents should be designed to target specific tissues or molecular markers, improving the specificity and sensitivity of SR-PAI. Nanotechnology and molecular engineering will play crucial roles in this endeavor. Continued exploration of nanoparticles, such as gold nanorods or carbon nanotubes for SR PAI is expected to offer high absorption, biocompatibility, tunability of optical properties, etc. Future research will likely also focus on developing multifunctional agents allowing for simultaneous diagnosis as well as treatment or providing signals for multiple imaging techniques, such as PAI combined with fluorescence or ultrasound imaging.

Finally, clinical translation will require rigorous validation and standardization of SR-PAI techniques. Large-scale preclinical studies and clinical trials are needed to demonstrate safety, efficacy, and reproducibility. Establishing standardized protocols and guidelines will facilitate regulatory approval and clinical adoption. We would like to point out that current SR-PAI works primarily focused on phantom and small animal studies to validate the efficacy and accuracy, which have paved

the groundwork for future translation from preclinical applications to clinical practice.

By addressing the outstanding challenges and pursuing new research directions, SR-PAI can evolve into a more robust and versatile imaging tool, capable of providing unprecedented insights into biological structures and processes at the molecular and cellular levels at unprecedented depths.

ACKNOWLEDGMENT

This work was partially sponsored by the United States National Institutes of Health (NIH) grants R21EB027981, R21 EB027304, RF1 NS115581, R01 NS111039, R01 EB028143, R01 DK139109; The United States National Science Foundation (NSF) CAREER award 2144788; Duke University Pratt Beyond the Horizon Grant; Eli Lilly Research Award Program; and Chan Zuckerberg Initiative Grant (2020-226178).

REFERENCES

[1] L. V. Wang, "Prospects of photoacoustic tomography," *Medical Physics,* vol. 35, no. 12, pp. 5758-5767, 2008, doi: https://doi.org/10.1118/1.3013698.

[2] L. V. Wang and S. Hu, "Photoacoustic Tomography: In Vivo Imaging from Organelles to Organs," *Science,* vol. 335, no. 6075, pp. 1458-1462, 2012, doi: doi:10.1126/science.1216210.

[3] J. Yao and L. V. Wang, "Photoacoustic microscopy," *Laser & Photonics Reviews,* vol. 7, no. 5, pp. 758-778, 2013, doi: https://doi.org/10.1002/lpor.201200060.

[4] S. Manohar and D. Razansky, "Photoacoustics: a historical review," *Adv. Opt. Photon.,* vol. 8, no. 4, pp. 586-617, 2016/12/31 2016, doi: 10.1364/AOP.8.000586.

[5] L. V. Wang and J. Yao, "A practical guide to photoacoustic tomography in the life sciences," *Nature Methods,* vol. 13, no. 8, pp. 627-638, 2016/08/01 2016, doi: 10.1038/nmeth.3925.

[6] L. V. Wang, "Multiscale photoacoustic microscopy and computed tomography," *Nature Photonics,* vol. 3, no. 9, pp. 503-509, 2009/09/01 2009, doi: 10.1038/nphoton.2009.157.

[7] K. Maslov, H. F. Zhang, S. Hu, and L. V. Wang, "Optical-resolution photoacoustic microscopy for in vivo imaging of single capillaries," *Optics Letters,* vol. 33, no. 9, pp. 929-931, 2008/05/01 2008, doi: 10.1364/OL.33.000929.

[8] H. F. Zhang, K. Maslov, G. Stoica, and L. V. Wang, "Functional photoacoustic microscopy for high-resolution and noninvasive in vivo imaging," *Nature Biotechnology,* vol. 24, no. 7, pp. 848-851, 2006/07/01 2006, doi: 10.1038/nbt1220.

[9] X. L. Déan-Ben and D. Razansky, "A practical guide for model-based reconstruction in optoacoustic imaging," *FRONTIERS IN PHYSICS,* vol. 10, NOV 1 2022, Art no. 1028258, doi: 10.3389/fphy.2022.1028258.

[10] M. J. Rust, M. Bates, and X. Zhuang, "Sub-diffraction-limit imaging by stochastic optical reconstruction microscopy (STORM)," *Nature Methods,* vol. 3, no. 10, pp. 793-796, 2006/10/01 2006, doi: 10.1038/nmeth929.

[11] E. Betzig *et al.*, "Imaging Intracellular Fluorescent Proteins at Nanometer Resolution," *Science,* vol. 313, no. 5793, pp. 1642-1645, 2006, doi: doi:10.1126/science.1127344.

[12] C. Errico *et al.*, "Ultrafast ultrasound localization microscopy for deep super-resolution vascular imaging," *Nature,* vol. 527, no. 7579, pp. 499-502, 2015/11/01 2015, doi: 10.1038/nature16066.

[13] X. L. Dean-Ben and D. Razansky, "Localization optoacoustic tomography," *LIGHT-SCIENCE & APPLICATIONS,* vol. 7, APR 20 2018, Art no. e18004, doi: 10.1038/lsa.2018.4.

[14] S. Vilov, B. Arnal, and E. Bossy, "Overcoming the acoustic diffraction limit in photoacoustic imaging by the localization of flowing absorbers," *OPTICS LETTERS,* vol. 42, no. 21, pp. 4379-4382, NOV 1 2017, doi: 10.1364/OL.42.004379.

[15] P. F. Zhang, L. Li, L. Lin, J. H. Shi, and L. H. V. Wang, "In vivo superresolution photoacoustic computed tomography by localization of single dyed droplets," *LIGHT-SCIENCE & APPLICATIONS,* vol. 8, APR 3 2019, Art no. 36, doi: 10.1038/s41377-019-0147-9.

[16] X. L. Deán-Ben *et al.*, "Deep optoacoustic localization microangiography of ischemic stroke in mice," *NATURE COMMUNICATIONS,* vol. 14, no. 1, JUN 16 2023, doi: 10.1038/s41467-023-39069-1.

[17] J. Kim, J. Y. Kim, S. Jeon, J. W. Baik, S. H. Cho, and C. Kim, "Super-resolution localization photoacoustic microscopy using intrinsic red blood cells as contrast absorbers," *LIGHT-SCIENCE & APPLICATIONS,* vol. 8, NOV 20 2019, Art no. 103, doi: 10.1038/s41377-019-0220-4.

[18] J. Kim *et al.*, "Deep learning alignment of bidirectional raster scanning in high speed photoacoustic microscopy," *SCIENTIFIC REPORTS,* vol. 12, no. 1, SEP 28 2022, Art no. 16238, doi: 10.1038/s41598-022-20378-2.

[19] Y. Li *et al.*, "Snapshot photoacoustic topography through an ergodic relay for high-throughput imaging of optical absorption," *Nature Photonics,* vol. 14, no. 3, pp. 164-170, 2020/03/01 2020, doi: 10.1038/s41566-019-0576-2.

[20] T. Dertinger, R. Colyer, G. Iyer, S. Weiss, and J. Enderlein, "Fast, background-free, 3D super-resolution optical fluctuation imaging (SOFI)," *Proceedings of the National Academy of Sciences,* vol. 106, no. 52, pp. 22287-22292, 2009, doi: doi:10.1073/pnas.0907866106.

[21] J.-E. Oh, Y.-W. Cho, G. Scarcelli, and Y.-H. Kim, "Sub-Rayleigh imaging via speckle illumination," *Optics Letters,* vol. 38, no. 5, pp. 682-684, 2013/03/01 2013, doi: 10.1364/OL.38.000682.

[22] J. Gateau, T. Chaigne, O. Katz, S. Gigan, and E. Bossy, "Improving visibility in photoacoustic imaging using dynamic speckle illumination," *Optics Letters,* vol. 38, no. 23, pp. 5188-5191, 2013/12/01 2013, doi: 10.1364/OL.38.005188.

[23] T. Chaigne *et al.*, "Super-resolution photoacoustic fluctuation imaging with multiple speckle illumination," *OPTICA,* vol. 3, no. 1, pp. 54-57, JAN 20 2016, doi: 10.1364/OPTICA.3.000054.

[24] T. W. Murray, M. Haltmeier, T. Berer, E. Leiss-Holzinger, and P. Burgholzer, "Super-resolution photoacoustic microscopy using blind structured illumination," *OPTICA,* vol. 4, no. 1, pp. 17-22, JAN 20 2017, doi: 10.1364/OPTICA.4.000017.

[25] P. H. Liu, "Label-free STORM principle realized by super-Rayleigh speckle in photoacoustic imaging," *OPTICS LETTERS,* vol. 44, no. 19, pp. 4642-4645, OCT 1 2019, doi: 10.1364/OL.44.004642.

[26] E. Hojman *et al.*, "Photoacoustic imaging beyond the acoustic diffraction-limit with dynamic speckle illumination and sparse joint support recovery," *OPTICS EXPRESS,* vol. 25, no. 5, pp. 4875-4886, MAR 6 2017, doi: 10.1364/OE.25.004875.

[27] T. Chaigne, B. Arnal, S. Vilov, E. Bossy, and O. Katz, "Super-resolution photoacoustic imaging via flow-induced absorption fluctuations," *OPTICA,* vol. 4, no. 11, pp. 1397-1404, NOV 20 2017, doi: 10.1364/OPTICA.4.001397.

[28] S. Vilov, G. Godefroy, B. Arnal, and E. Bossy, "Photoacoustic fluctuation imaging: theory and application to blood flow imaging," *Optica,* vol. 7, no. 11, pp. 1495-1505, 2020/11/20 2020, doi: 10.1364/OPTICA.400517.

[29] G. Godefroy, B. Arnal, and E. Bossy, "Full-visibility 3D imaging of oxygenation and blood flow by simultaneous multispectral photoacoustic fluctuation imaging (MS-PAFI) and ultrasound Doppler," *Scientific Reports,* vol. 13, no. 1, p. 2961, 2023/02/20 2023, doi: 10.1038/s41598-023-29177-9.

[30] M. G. L. Gustafsson, "Surpassing the lateral resolution limit by a factor of two using structured illumination microscopy," *Journal of Microscopy,* vol. 198, no. 2, pp. 82-87, 2000, doi: https://doi.org/10.1046/j.1365-2818.2000.00710.x.

[31] B.-J. Chang, V. D. Perez Meza, and E. H. K. Stelzer, "csiLSFM combines light-sheet fluorescence microscopy and coherent structured illumination for a lateral resolution below 100 nm," *Proceedings of the National Academy of Sciences,* vol. 114, no. 19, pp. 4869-4874, 2017, doi: doi:10.1073/pnas.1609278114.

[32] J. Liang, L. Gao, C. Li, and L. V. Wang, "Spatially Fourier-encoded photoacoustic microscopy using a digital micromirror device," *Optics Letters,* vol. 39, no. 3, pp. 430-433, 2014/02/01 2014, doi: 10.1364/OL.39.000430.

[33] Hanley, Verveer, Arndt-Jovin, and Jovin, "Three-dimensional spectral imaging by Hadamard transform spectroscopy in a programmable array microscope," *Journal of Microscopy,* vol. 197, no. 1, pp. 5-14, 2000, doi: https://doi.org/10.1046/j.1365-2818.2000.00665.x.

[34] J. Yang *et al.*, "Motionless volumetric photoacoustic microscopy with spatially invariant resolution," *Nature Communications,* vol. 8, no. 1, p. 780, 2017/10/03 2017, doi: 10.1038/s41467-017-00856-2.

[35] M. Amjadian, S. M. Mostafavi, J. B. Chen, Z. Kavehvash, J. Y. Zhu, and L. D. Wang, "Super-Resolution Photoacoustic Microscopy Using Structured-Illumination," *IEEE TRANSACTIONS ON MEDICAL IMAGING,* vol. 40, no. 9, pp. 2197-2207, SEP 2021, doi: 10.1109/TMI.2021.3073555.

[36] M. Amjadian, S. M. Mostafavi, Z. Kavehvash, and R. Faez, "Fast three-dimensional super-resolution photoacoustic microscopy imaging," *OPTICAL ENGINEERING,* vol. 60, no. 12, DEC 2021, Art no. 123108, doi: 10.1117/1.OE.60.12.123108.

[37] M. Amjadian, S. M. Mostafavi, J. B. Chen, L. D. Wang, and Z. T. Luo, "Super-Resolution Photoacoustic Microscopy via Modified Phase Compounding," *IEEE TRANSACTIONS ON MEDICAL IMAGING,* vol. 41, no. 11, pp. 3411-3420, NOV 2022, doi: 10.1109/TMI.2022.3184711.

[38] Z. Chen, A. Özbek, J. Rebling, Q. Zhou, X. L. Deán-Ben, and D. Razansky, "Multifocal structured illumination optoacoustic microscopy," *Light: Science & Applications,* vol. 9, no. 1, p. 152, 2020/08/31 2020, doi: 10.1038/s41377-020-00390-9.

[39] B. Park, H. Lee, S. Jeon, J. Ahn, H. H. Kim, and C. Kim, "Reflection-mode switchable subwavelength Bessel-beam and Gaussian-beam photoacoustic microscopy in vivo," *Journal of Biophotonics,* vol. 12, no. 2, p. e201800215, 2019, doi: https://doi.org/10.1002/jbio.201800215.

[40] B. Jiang, X. Yang, and Q. Luo, "Reflection-mode Bessel-beam photoacoustic microscopy for in vivo imaging of cerebral capillaries," *Optics Express,* vol. 24, no. 18, pp. 20167-20176, 2016/09/05 2016, doi: 10.1364/OE.24.020167.

[41] J. Shi, L. Wang, C. Noordam, and L. Wang, "Bessel-beam Grueneisen relaxation photoacoustic microscopy with extended depth of field," *Journal of Biomedical Optics,* vol. 20, no. 11, p. 116002, 2015. [Online]. Available: https://doi.org/10.1117/1.JBO.20.11.116002.

[42] C. Yeh, B. Soetikno, S. Hu, K. Maslov, and L. Wang, "Microvascular quantification based on contour-scanning photoacoustic microscopy," *Journal of Biomedical Optics,* vol. 19, no. 9, p. 096011, 2014. [Online]. Available: https://doi.org/10.1117/1.JBO.19.9.096011.

[43] W. Kim, C. Lee, C. Kim, and D. S. Kim, "Dual-mode reconfigurable focusing using the interface of aqueous and dielectric liquids," *Lab on a Chip,* vol. 17, no. 23, pp. 4031-4039, 2017.

[44] X. Yang, B. Jiang, X. Song, J. Wei, and Q. Luo, "Fast axial-scanning photoacoustic microscopy using tunable acoustic gradient lens," *Optics Express,* vol.

25, no. 7, pp. 7349-7357, 2017/04/03 2017, doi: 10.1364/OE.25.007349.

[45] M. Jiang, X. Zhang, C. A. Puliafito, H. F. Zhang, and S. Jiao, "Adaptive optics photoacoustic microscopy," *Optics Express,* vol. 18, no. 21, pp. 21770-21776, 2010/10/11 2010, doi: 10.1364/OE.18.021770.

[46] A. M. Caravaca-Aguirre, D. B. Conkey, J. D. Dove, H. Ju, T. W. Murray, and R. Piestun, "High contrast three-dimensional photoacoustic imaging through scattering media by localized optical fluence enhancement," *Optics Express,* vol. 21, no. 22, pp. 26671-26676, 2013/11/04 2013, doi: 10.1364/OE.21.026671.

[47] D. B. Conkey, A. M. Caravaca-Aguirre, J. D. Dove, H. Y. Ju, T. W. Murray, and R. Piestun, "Super-resolution photoacoustic imaging through a scattering wall," *NATURE COMMUNICATIONS,* vol. 6, AUG 2015, Art no. 7902, doi: 10.1038/ncomms8902.

[48] Y. Notsuka, M. Kurihara, N. Hashimoto, Y. Harada, E. Takahashi, and Y. Yamaoka, "Improvement of spatial resolution in photoacoustic microscopy using transmissive adaptive optics with a low-frequency ultrasound transducer," *Optics Express,* vol. 30, no. 2, pp. 2933-2948, 2022/01/17 2022, doi: 10.1364/OE.446309.

[49] Y. Shen *et al.*, "Acoustic-feedback wavefront-adapted photoacoustic microscopy," *Optica,* vol. 11, no. 2, pp. 214-221, 2024/02/20 2024, doi: 10.1364/OPTICA.511359.

[50] A. C. Stiel, X. L. Deán-Ben, Y. Jiang, V. Ntziachristos, D. Razansky, and G. G. Westmeyer, "High-contrast imaging of reversibly switchable fluorescent proteins via temporally unmixed multispectral optoacoustic tomography," *Optics Letters,* vol. 40, no. 3, pp. 367-370, 2015/02/01 2015, doi: 10.1364/OL.40.000367.

[51] J. Yao *et al.*, "Multiscale photoacoustic tomography using reversibly switchable bacterial phytochrome as a near-infrared photochromic probe," *Nature Methods,* vol. 13, no. 1, pp. 67-73, 2016/01/01 2016, doi: 10.1038/nmeth.3656.

[52] L. Wang, C. Zhang, and L. V. Wang, "Grueneisen Relaxation Photoacoustic Microscopy," *Physical Review Letters,* vol. 113, no. 17, p. 174301, 10/20/ 2014, doi: 10.1103/PhysRevLett.113.174301.

[53] J. Ma, J. Shi, P. Hai, Y. Zhou, and L. Wang, "Grueneisen relaxation photoacoustic microscopy in vivo," *Journal of Biomedical Optics,* vol. 21, no. 6, p. 066005, 2016. [Online]. Available: https://doi.org/10.1117/1.JBO.21.6.066005 https://www.ncbi.nlm.nih.gov/pmc/articles/PMC4897030/pdf/JBO-021-066005.pdf.

[54] X. Liu, T. T. W. Wong, J. Shi, J. Ma, Q. Yang, and L. V. Wang, "Label-free cell nuclear imaging by Grüneisen relaxation photoacoustic microscopy," *Optics Letters,* vol. 43, no. 4, pp. 947-950, 2018/02/15 2018, doi: 10.1364/OL.43.000947.

[55] J. Shi *et al.*, "High-resolution, high-contrast mid-infrared imaging of fresh biological samples with ultraviolet-localized photoacoustic microscopy," *Nature Photonics,* vol. 13, no. 9, pp. 609-615, 2019/09/01 2019, doi: 10.1038/s41566-019-0441-3.

[56] J. Shi *et al.*, "Grüneisen-relaxation photoacoustic microscopy at 1.7 µm and its application in lipid imaging," *Optics Letters,* vol. 45, no. 12, pp. 3268-3271, 2020/06/15 2020, doi: 10.1364/OL.393780.

[57] J. Yao, L. Wang, C. Li, C. Zhang, and L. V. Wang, "Photoimprint Photoacoustic Microscopy for Three-Dimensional Label-Free Subdiffraction Imaging," *Physical Review Letters,* vol. 112, no. 1, p. 014302, 01/10/ 2014, doi: 10.1103/PhysRevLett.112.014302.

[58] W. Yi, X. Da, Z. Yaguang, and C. Qun, "Photoacoustic imaging with deconvolution algorithm," *Physics in Medicine & Biology,* vol. 49, no. 14, p. 3117, 2004/06/28 2004, doi: 10.1088/0031-9155/49/14/006.

[59] C. Zhang, K. Maslov, J. Yao, and L. Wang, "In vivo photoacoustic microscopy with 7.6-µm axial resolution using a commercial 125-MHz ultrasonic transducer," *Journal of Biomedical Optics,* vol. 17, no. 11, p. 116016, 2012. [Online]. Available: https://doi.org/10.1117/1.JBO.17.11.116016.

[60] D. Cai, Z. Li, Y. Li, Z. Guo, and S.-L. Chen, "Photoacoustic microscopy in vivo using synthetic-aperture focusing technique combined with three-dimensional deconvolution," *Optics Express,* vol. 25, no. 2, pp. 1421-1434, 2017/01/23 2017, doi: 10.1364/OE.25.001421.

[61] D. Cai, Z. Li, and S.-L. Chen, "In vivo deconvolution acoustic-resolution photoacoustic microscopy in three dimensions," *Biomed. Opt. Express,* vol. 7, no. 2, pp. 369-380, 2016/02/01 2016, doi: 10.1364/BOE.7.000369.

[62] H. Jin, R. Zhang, S. Liu, and Y. Zheng, "Fast and High-Resolution Three-Dimensional Hybrid-Domain Photoacoustic Imaging Incorporating Analytical-Focused Transducer Beam Amplitude," *IEEE Transactions on Medical Imaging,* vol. 38, no. 12, pp. 2926-2936, 2019, doi: 10.1109/TMI.2019.2917688.

[63] J. Chen, R. Lin, H. Wang, J. Meng, H. Zheng, and L. Song, "Blind-deconvolution optical-resolution photoacoustic microscopy in vivo," *Optics Express,* vol. 21, no. 6, pp. 7316-7327, 2013/03/25 2013, doi: 10.1364/OE.21.007316.

[64] F. Feng, S. Q. Liang, J. J. Luo, and S. L. Chen, "High-fidelity deconvolution for acoustic-resolution photoacoustic microscopy enabled by convolutional neural networks," *PHOTOACOUSTICS,* vol. 26, JUN 2022, Art no. 100360, doi: 10.1016/j.pacs.2022.100360.

[65] S. Jeon, J. Kim, D. Lee, J. W. Baik, and C. Kim, "Review on practical photoacoustic microscopy," *Photoacoustics,* vol. 15, p. 100141, 2019/09/01/ 2019, doi: https://doi.org/10.1016/j.pacs.2019.100141.

[66] M.-L. Li, H. F. Zhang, K. Maslov, G. Stoica, and L. V. Wang, "Improved in vivo photoacoustic microscopy based on a virtual-detector concept,"

Optics Letters, vol. 31, no. 4, pp. 474-476, 2006/02/15 2006, doi: 10.1364/OL.31.000474.

[67] J. Park, S. Jeon, J. Meng, L. Song, J. Lee, and C. Kim, "Delay-multiply-and-sum-based synthetic aperture focusing in photoacoustic microscopy," *Journal of Biomedical Optics,* vol. 21, no. 3, p. 036010, 2016. [Online]. Available: https://doi.org/10.1117/1.JBO.21.3.036010.

[68] Z. Deng, X. Yang, H. Gong, and Q. Luo, "Two-dimensional synthetic-aperture focusing technique in photoacoustic microscopy," *Journal of Applied Physics,* vol. 109, no. 10, 2011, doi: 10.1063/1.3585828.

[69] J. Turner, H. Estrada, M. Kneipp, and D. Razansky, "Improved optoacoustic microscopy through three-dimensional spatial impulse response synthetic aperture focusing technique," *Optics Letters,* vol. 39, no. 12, pp. 3390-3393, 2014/06/15 2014, doi: 10.1364/OL.39.003390.

[70] Z. Deng, X. Yang, H. Gong, and Q. Luo, "Adaptive synthetic-aperture focusing technique for microvasculature imaging using photoacoustic microscopy," *Optics Express,* vol. 20, no. 7, pp. 7555-7563, 2012/03/26 2012, doi: 10.1364/OE.20.007555.

[71] S. Jeon, J. Park, R. Managuli, and C. Kim, "A Novel 2-D Synthetic Aperture Focusing Technique for Acoustic-Resolution Photoacoustic Microscopy," *IEEE Transactions on Medical Imaging,* vol. 38, no. 1, pp. 250-260, 2019, doi: 10.1109/TMI.2018.2861400.

[72] B. Huang *et al.*, "Enhancing image resolution of confocal fluorescence microscopy with deep learning," *PhotoniX,* vol. 4, no. 1, p. 2, 2023/01/05 2023, doi: 10.1186/s43074-022-00077-x.

[73] Y. He *et al.*, "Self-supervised deep-learning two-photon microscopy," *Photon. Res.,* vol. 11, no. 1, pp. 1-11, 2023/01/01 2023, doi: 10.1364/PRJ.469231.

[74] H. Wang *et al.*, "Deep learning enables cross-modality super-resolution in fluorescence microscopy," *Nature Methods,* vol. 16, no. 1, pp. 103-110, 2019/01/01 2019, doi: 10.1038/s41592-018-0239-0.

[75] Z. Yuan, D. Yang, W. Wang, J. Zhao, and Y. Liang, "Self super-resolution of optical coherence tomography images based on deep learning," *Optics Express,* vol. 31, no. 17, pp. 27566-27581, 2023/08/14 2023, doi: 10.1364/OE.495530.

[76] N. Awasthi, G. Jain, S. K. Kalva, M. Pramanik, and P. K. Yalavarthy, "Deep Neural Network-Based Sinogram Super-Resolution and Bandwidth Enhancement for Limited-Data Photoacoustic Tomography," *IEEE TRANSACTIONS ON ULTRASONICS FERROELECTRICS AND FREQUENCY CONTROL,* vol. 67, no. 12, pp. 2660-2673, DEC 2020, doi: 10.1109/TUFFC.2020.2977210.

[77] Z. Zhang *et al.*, "Adaptive enhancement of acoustic resolution photoacoustic microscopy imaging via deep CNN prior," *Photoacoustics,* vol. 30, p. 100484, 2023/04/01/ 2023, doi: https://doi.org/10.1016/j.pacs.2023.100484.